Available online at www.sciencedirect.com
SCIENCE DIRECT®
ELSEVIER
Palaeogeography, Palaeoclimatology, Palaeoecology 207 (2004) 127–141
PALAEO
www.elsevier.com/locate/palaeo

Sensitivity of the ocean–atmosphere carbon cycle to ice-covered and ice-free conditions in the Nordic Seas during the Last Glacial Maximum

Michael Schulz[a,b,*], André Paul[b]

[a] Institut für Geowissenschaften, Universität Kiel, D-24098 Kiel, Germany
[b] Fachbereich Geowissenschaften and DFG Forschungszentrum "Ozeanränder", Universität Bremen, D-28334 Bremen, Germany

Abstract

A global carbon-cycle box model forced by an ocean-general circulation model (OGCM) is used to investigate how different sea-surface reconstructions for the northern North Atlantic Ocean (Nordic Seas) for the Last Glacial Maximum (LGM) affect the ocean–atmosphere carbon cycle via changes in the large-scale thermohaline circulation. For perennial sea-ice cover in the Nordic Seas [CLIMAP, Chart Ser. (Geol. Soc. Am.) MC-36 (1981)], the model-predicted deep-water formation areas, $\delta^{13}C$ distribution and ^{14}C ventilation ages are partly inconsistent with palaeoceanographic data for the glacial Atlantic Ocean. Considering ice-free conditions during LGM summer in the Nordic Seas [Weinelt et al., Palaeoclimatology 1 (1996) 283] brings the model results in better agreement with palaeoceanographic findings, thus supporting this particular sea-surface reconstruction. For both LGM scenarios, the ocean circulation model simulates a reduction in the export of North Atlantic Deep Water (NADW) to the Southern Ocean by 50% compared to today. The effect of changes in the intensity of the thermohaline circulation on atmospheric CO_2 content alone is rather small, accounting for approximately 20% of the net CO_2 lowering during the LGM.

Keywords: Thermohaline circulation; North Atlantic Deep Water; Carbon isotopes; Ventilation age; Ocean-general circulation model; Carbon-cycle model

1. Introduction

Two widely accepted lines of evidence suggest that the operation of the global carbon cycle differed between today and the Last Glacial Maximum (LGM; 18.0–21.5 thousand calendar years before present; Sarnthein et al., 2001): (i) glacial atmospheric CO_2 partial pressure (pCO_2) was lowered by 80 μatm (Barnola et al., 1987) and (ii) stable carbon isotope ratios ($\delta^{13}C$) measured on benthic foraminifera from deep-sea sediments reveal pronounced shifts in ventilation of deep and intermediate water masses of the global ocean (Boyle and Keigwin, 1987; Curry et al., 1988; Duplessy et al., 1988; Sarnthein et al., 1994). In particular, the $\delta^{13}C$ data suggest a reduction in North Atlantic Deep Water (NADW) formation during the LGM. During the past two decades, a variety of mechanisms have been suggested to explain the

* Corresponding author. Fachbereich Geowissenschaften and DFG Forschungszentrum "Ozeanränder", Universität Bremen, Postfach 330 440, D-28334 Bremen, Germany. Tel.: +49-421-218-7136; fax: +49-421-218-7040.
E-mail address: mschulz@palmod.uni-bremen.de (M. Schulz).

0031-0182/$ - see front matter © 2004 Elsevier B.V. All rights reserved.
doi:10.1016/j.palaeo.2004.02.005

glacial pCO_2 lowering and the concomitant changes in oceanic $\delta^{13}C$ distribution. However, none of the mechanisms proposed so far has been generally accepted (summaries in Archer et al., 2000; Sigman and Boyle, 2000).

Different classes of models have been used to understand the possible effect of changes in the large-scale oceanic thermohaline circulation on the ocean–atmosphere carbon cycle: While many box-model studies, employing prescribed changes in ocean circulation, resulted in pCO_2 reductions between 8 and 67 μatm upon a prescribed decrease in ocean mixing rates (Siegenthaler and Wenk, 1984; Broecker and Peng, 1986; Boyle, 1988; Keir, 1988; Toggweiler, 1999; Stephens and Keeling, 2000) only few experiments led also to reasonable changes in oceanic $\delta^{13}C$ distribution (Keir, 1990; Toggweiler, 1999). A problem of all these studies is that the water fluxes between the boxes for both modern and LGM state are tunable model parameters, that is, they are free of dynamic constraints. In contrast to these studies, experiments with a 3D biogeochemical model, which resolves the dynamics of the oceanic circulation explicitly, resulted only in a marginal pCO_2 drop of 6 μatm for an LGM circulation pattern being largely consistent with the reconstructed $\delta^{13}C$ distributions (Winguth et al., 1999).

Ocean circulation studies for the LGM have been conducted with 3D ocean-general circulation models (OGCM) using reconstructed LGM sea-surface conditions (Seidov and Haupt, 1999; Campin et al., 1999; Schäfer-Neth and Paul, 2001; Paul and Schäfer-Neth, 2003) as well as with coupled atmosphere–ocean models of different complexity (Ganopolski et al., 1998; Weaver et al., 1998; Hewitt et al., 2001; Kim et al., 2002). Only some of the resulting circulation fields, which are dynamically consistent, have been used to force global biogeochemical models (Archer et al., 2000; Schulz et al., 2001; Brovkin et al., 2002). Schulz et al. (2001) used the OGCM results of Seidov and Haupt (1999) to quantify changes in ocean–atmosphere carbon budgets during the initial phase of the last deglaciation. However, the interpretation of the results was limited by the low, basin-scale resolution of the employed biogeochemical model. Here, we use an improved version of this biogeochemical model, with increased horizontal resolution, to study the global carbon cycle during the LGM.

Our strategy is to force a global OGCM with LGM sea-surface conditions, derived from palaeoceanographic reconstructions, and to use the resulting OGCM output to force a global biogeochemical model. For the greater part of the global ocean, we use the sea-surface temperature (SST) reconstructions of CLIMAP (1981). An important feature of this reconstruction is a perennial sea-ice cover in the Nordic Seas, that is, the modern sites of NADW production. In contrast to the CLIMAP (1981) reconstruction, a recent SST reconstruction suggested ice-free conditions during LGM summer in this region (Weinelt et al., 1996). The purpose of this study is to investigate how these different palaeoceanographic reconstructions affect the ocean–atmosphere carbon cycle through changes in the large-scale thermohaline circulation of the ocean. Our study aims not at explaining the observed atmospheric pCO_2 difference between today and the LGM. (Throughout the text we use the term modern/today as a synonym for preindustrial with respect to the carbon cycle and for present-day with respect to the ocean circulation.)

2. Model setup

2.1. Ocean model

We use a modified version of the Hamburg Large-Scale Geostrophic (LSG) ocean model (Maier-Reimer et al., 1993) in a global configuration with an average horizontal resolution of 3.5° and 11 layers in the vertical. The most important modification to the LSG ocean model is the implementation of a new tracer advection scheme (after Farrow and Stevens, 1995), which is significantly less diffusive than the upwind scheme used in the original model. Further modifications include a new convection scheme, explicit vertical diffusion, and depth-dependent horizontal and vertical diffusivities. The model is forced by restoring temperature and salinity at the sea surface to either observed modern or reconstructed LGM values. Sea-ice extent is prescribed and the restoring SST in sea-ice-covered grid cells is set to the freezing point of seawater (-1.8 °C). Details of the model setup are given by Schäfer-Neth and Paul (2001).

Apart from the modern control experiment (CTRL; Table 1), two LGM experiments were conducted, one based on CLIMAP (1981) sea-surface conditions with perennial ice cover in the Nordic Seas (experiment LGMC) and the other taking into account the ice-free conditions in the Nordic Seas during summer (Weinelt et al., 1996; experiment LGMW). For experiment LGMC, a seasonal SST cycle was constructed by fitting a sinusoid through the February and August data given by CLIMAP (1981). This seasonal SST cycle was refined by a plausible seasonal cycle for sea-ice extent, with the extremes given by the CLIMAP sea-ice reconstructions for February and August. For experiment LGMW, the SST reconstructions for the northern North Atlantic were merged with the original CLIMAP SST reconstruction for the world ocean. Sea-surface salinities (SSS) for both LGM experiments were derived from reconstructed SST and oxygen-isotope ratios ($\delta^{18}O$) measured on sedimentary planktonic foraminifera (Duplessy et al., 1991) using a $\delta^{18}O$:SSS ratio of 1:1.8 (Schäfer-Neth and Paul, 2001 for further details). Finally, wind stress was taken from the response of the atmospheric general circulation model ECHAM 3 to LGM boundary conditions (Lorenz et al., 1996). For all experiments the OGCM was integrated for more than 6000 years to reach a steady state.

Table 1
Data used for surface forcing of the OGCM in the three experiments (SST: sea-surface temperature, SSS: sea-surface salinity)

Experiment	Forcing data	
CTRL	SST	Shea et al. (1990); set to −1.8 °C in sea-ice covered regions
	SSS	Levitus et al. (1994); winter SSS in Ross/Weddell Seas after Johns et al. (1997)
	Wind	Lorenz et al. (1996)
LGMC	SST	CLIMAP (1981)
	SSS	via $\delta^{18}O$/SSS = 1:1.8 in the North Atlantic; SSS in Ross/Weddell Seas after Melles (1991); global anomaly of 1.08 psu elsewhere
	Wind	Lorenz et al. (1996)
LGMW	SST	Weinelt et al. (1996) in the North Atlantic; CLIMAP (1981) elsewhere
	SSS	as for LGMC but using Weinelt et al. SST for $\delta^{18}O$-to-SSS conversion
	Wind	Lorenz et al. (1996)

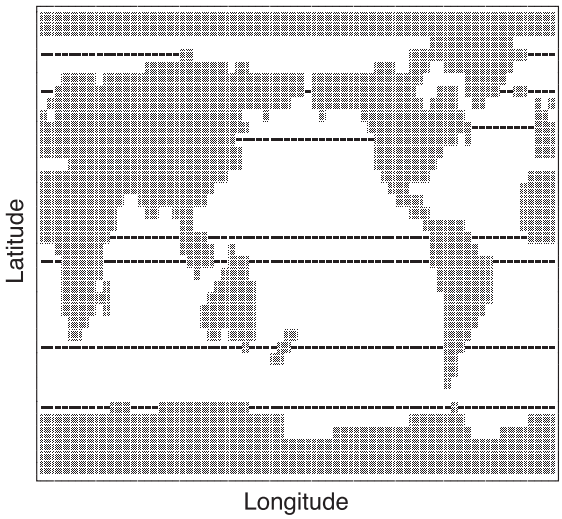

Fig. 1. Land-sea distribution in the OGCM and boundaries of box stacks in the carbon-cycle box model (solid lines).

2.2. Carbon-cycle model

The carbon-cycle model is realized as box model which is forced by annual-mean fields from the OGCM and is an improved version of the model used by Schulz et al. (2001). The model consists of an atmospheric box and 15 oceanic box stacks, each containing a surface box and 10 subsurface boxes with interface depths identical to the OGCM levels. Boundaries of the box stacks are selected such that the major oceanographic regions in each ocean basin are resolved (Fig. 1). Following basic box-modeling concepts (e. g. Keeling and Bolin, 1967; Bolin, 1981), the model predicts the concentrations of total dissolved inorganic carbon (DIC), stable ($DI^{13}C$) and radioactive ($DI^{14}C$) carbon isotopes, total alkalinity (ALK) and phosphate (PO_4) in the ocean. Oceanic tracer inventories are based on GEOSECS data (Takahashi et al., 1981) and are kept constant in all experiments.

Net water transports between the boxes are obtained by integration of the OGCM velocities over the box boundaries. Oceanic mixing processes are

explicitly included in the box model: Vertical mixing due to permanent circulation cells is given by the individually summed upward and downward transports in the OGCM across each depth-interface of the box model, whereas vertical tracer transport by eddies is parameterized by vertical diffusion with depth-dependent diffusivity (after Bryan and Lewis, 1979). Convection is parameterized as continuous mixing process between adjacent boxes, with mixing intensity proportional to the number of convective adjustment events per year in the OGCM (Bacastow and Maier-Reimer, 1990). Basin scale horizontal mixing is represented by depth-dependent horizontal diffusion (after Stocker et al., 1994).

In the atmospheric box partial pressures of total CO_2 (pCO_2) and carbon isotopes ($p^{13}CO_2$ and $p^{14}CO_2$) are predicted. The exchange of carbon across the ocean–atmosphere boundary is parameterized as linear gradient flux, taking into account isotopic fractionation (Zhang et al., 1995). Aqueous pCO_2 in the surface layer is determined after Peng et al. (1987) using the equilibrium constants for the dissociation of carbonic acid of Dickson and Millero (1987) (cf. Johnson et al., 1999). Temperatures and salinities of the topmost OGCM layer, averaged over the box-stack regions, are employed to calculate temperature-and salinity-dependent parameters in the box model. The surface freshwater fluxes diagnosed from the OGCM directly control the volume of the surface boxes, thus avoiding normalization of tracer concentrations to mean ocean salinity prior to calculating aqueous pCO_2. Gas-exchange coefficients increase nonlinearly with wind speed (Heimann and Monfray, 1989), as derived from the average wind stress over each box stack, and decrease linearly with increasing sea ice cover. For sea-ice cover above 90% gas exchange is held constant at 10% of its "ice-free value" to account for ice leads and polynyas. The atmosphere exchanges ^{12}C, ^{13}C and ^{14}C with a simple terrestrial biosphere (after Oeschger et al., 1975) using an exchange rate for total carbon which was held constant in all experiments.

Biological export production in the surface layers (Q_{bio}) occurs at a constant "Redfield ratio" (Anderson and Sarmiento, 1994) and is limited by the availability of PO_4. For the modern control experiment, export production in each surface layer is diagnosed by restoring PO_4 concentrations ($[PO_4]$) to observed values ($[PO_4]_{obs}$) (Najjar et al., 1992):

$$Q_{bio} = \frac{r_{C:P}}{\tau}([PO_4] - [PO_4]_{obs})V, \quad (1)$$

where $r_{C:P} = 117$ is the molar Redfield ratio between carbon and phosphate, $\tau = 0.1$ year is a restoring time scale and V denotes the volume of a surface layer. In contrast, export production in palaeoclimate experiments depend on PO_4 concentration according to Michaelis–Menten kinetics (Dugdale, 1967):

$$Q_{bio} = r_{C:P}\frac{\omega[PO_4]}{k_m + [PO_4]}, \quad (2)$$

with phosphate uptake rate ω and $k_m = 2.5 \cdot 10^{-4}$ mol m^{-3} (Lalli and Parsons, 1993). After determining export production from Eq. (1) for the modern control run, ω is derived from Eq. (2) and held fixed in the LGM experiments. The production ratio between calcareous shells and organic matter varies with temperature (after Heinze, 1990) and the isotopic composition of organic matter depends on ambient CO_2 concentration (Jasper et al., 1994). Since the model contains no sediment reservoir, all particles leaving the surface layer are remineralized at depth, using different depth scales for remineralization of organic matter and calcareous shells. In the modern control experiment, production of organic matter amounts to 11.1 and 1.25 Gt C $year^{-1}$ leave the surface ocean in biogenic carbonate shells, in harmony with recent estimates (11–16 Gt C $year^{-1}$ for organic matter (Falkowski et al., 2000) and 0.5–2.0 Gt C $year^{-1}$ for carbonate (Iglesias-Rodriguez et al., 2002)). The model was integrated for 80,000 years for the control experiment, while the LGM experiments were integrated for 20,000 years using the control run as initial condition.

3. Ocean modelling results

Modern zonally integrated meridional overturning is in good agreement with the deduced large-scale circulation pattern of the modern oceans. In the Atlantic Ocean (Fig. 2a), NADW is produced at a rate of 13 Sv (1 Sv = 10^6 m^3 s^{-1}), 4 Sv of which are derived from combined overflows through Denmark Strait and the

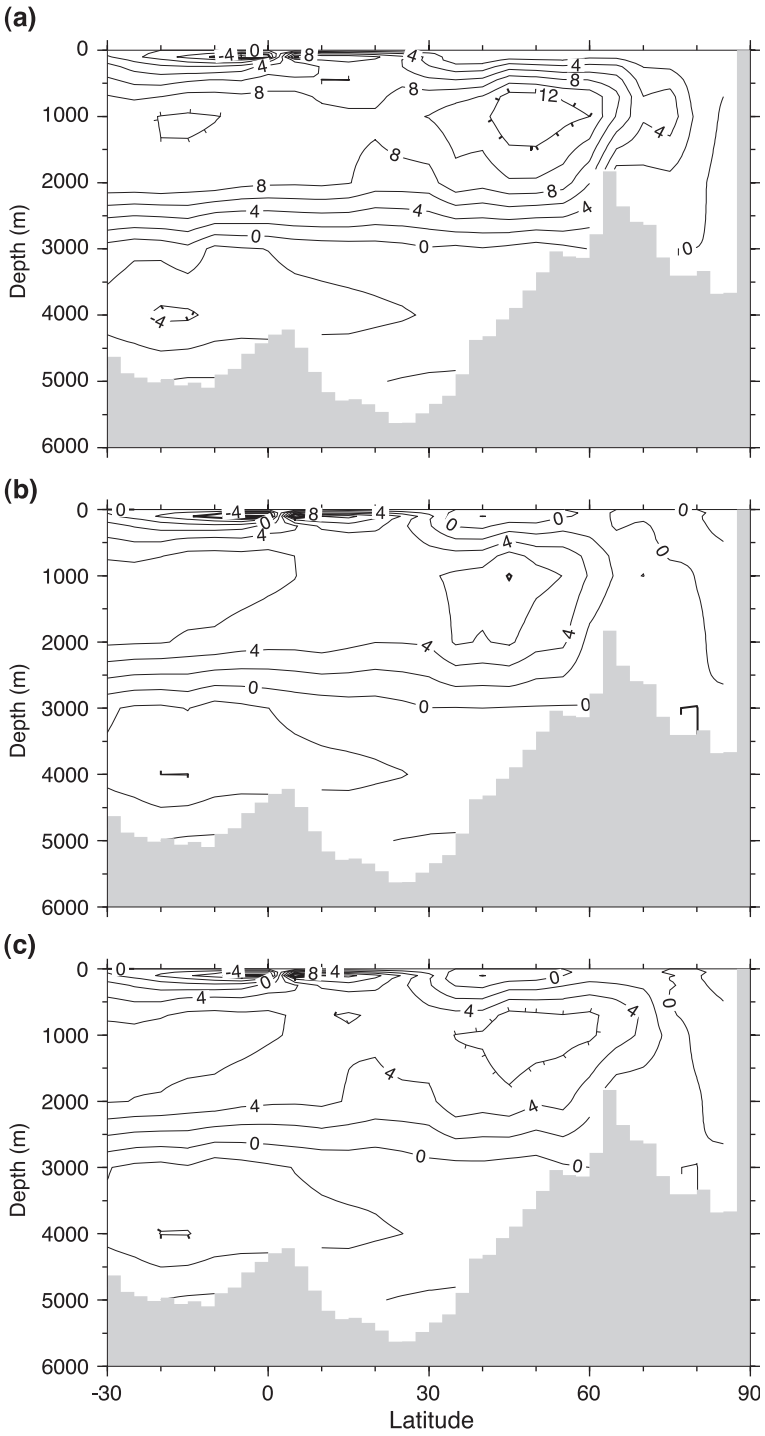

Fig. 2. Annual-mean meridional overturning stream function for the Atlantic Ocean in experiments (a) CTRL, (b) LGMC and (c) LGMW. Contours in [Sv] (1 Sv = 10^6 m^3 s^{-1}); positive values denote clockwise rotation.

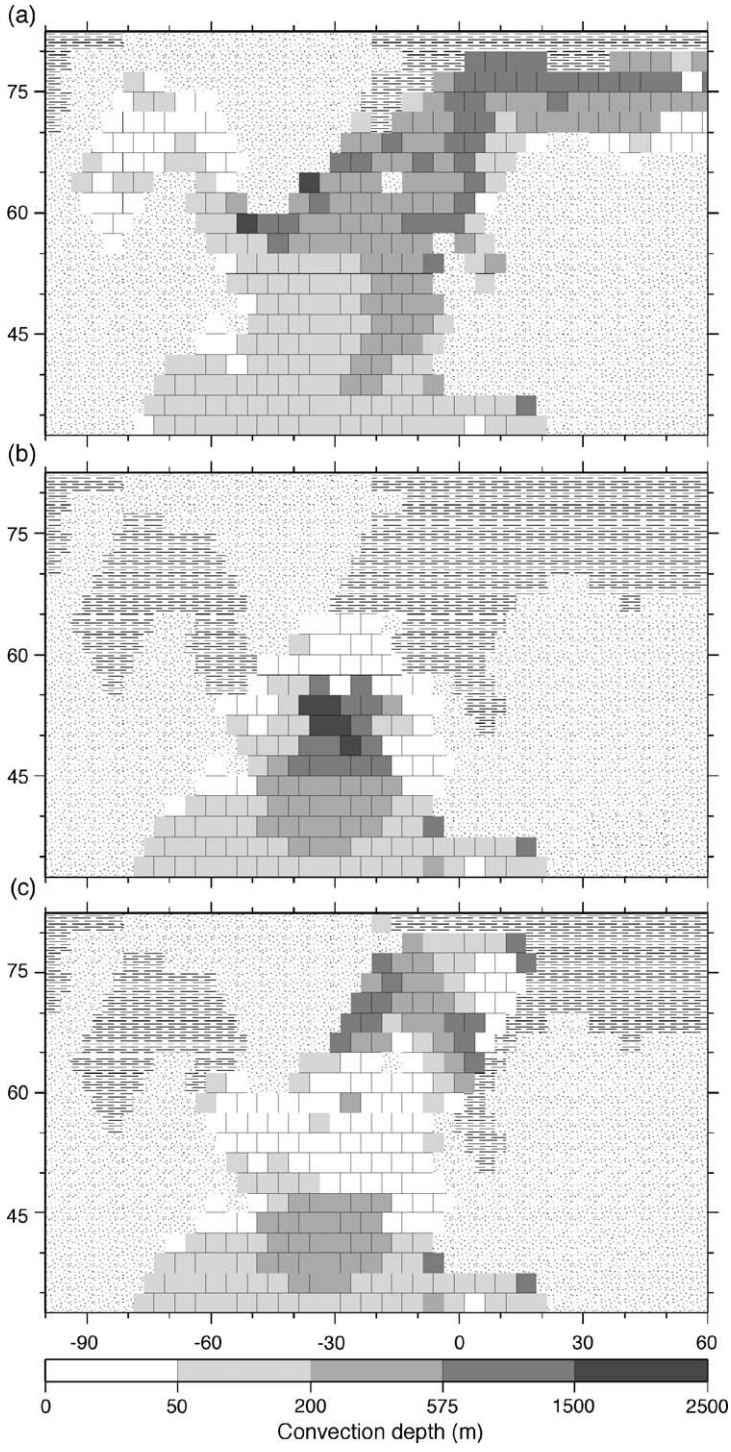

Fig. 3. Annual-mean convection depth (gray scale) and sea-ice extent (dashed) in the North Atlantic Ocean in experiments (a) CTRL, (b) LGMC and (c) LGMW. Dotted areas indicate land.

Iceland–Faeroe–Channel linked to convection in the Nordic Seas (Fig. 3a). Approximately 8 Sv of the newly formed NADW are exported (across 30°S) to the Southern Ocean at depths below 1.5 km. There is a deep inflow of Antarctic Bottom Water (AABW) amounting to ~4 Sv, which is compensated by a return flow of "modified AABW" above 3.5-km depth. Thus, the total amount of deep water ("pure recently formed NADW" and "modified AABW") which flows into the Southern Ocean is ~12 Sv, one-third less than the oceanographic estimate of 18 Sv (Schmitz, 1995). Moreover, the NADW/AABW water-mass boundary occurs ~1 km (or one model-layer thickness) too shallow in the model compared to observations (cf. Schäfer-Neth and Paul, 2001). A further discussion of the control experiment is provided by Schäfer-Neth and Paul (2001).

In experiment, LGMC the meridional overturning pattern in the Atlantic Ocean (Fig. 2b) shows the same basic structure as in the control experiment (Fig. 2a), including NADW formation and bottom water inflow from the Southern Ocean. NADW production and export to the Southern Ocean are reduced by 50% compared to the modern control experiment. This reduction goes along with a southward shift in NADW production sites from the Nordic Seas to locations south of Iceland (Fig. 3b). Also the wind-driven subtropical circulation cell in the North Atlantic Ocean expands (Seidov et al., 1996). In the zonal mean, the boundary between the deep current system and the bottom current system is only slightly shallower than in experiment CTRL, probably because the NADW cell is too shallow from the outset. AABW inflow still amounts to ~4 Sv.

Compared to experiment LGMC the ice-free conditions during LGM summer in experiment LGMW lead to a pronounced northward shift of the convection sites in the North Atlantic (cf. Fig. 3b,c), which leads to an increase in overflow across the Greenland-Scotland Ridge from ~1 (Fig. 2b) to ~4 Sv (Fig. 2c). Despite these changes, the effect of the seasonally ice-free Nordic Seas on the production rate of NADW and its export to the Southern Ocean is almost negligible (cf. Fig. 2b,c). Similarly, the amount of AABW flowing into the Atlantic Ocean is largely unaffected by the modified sea-surface conditions in the Nordic Seas (cf. Fig. 2b,c).

4. Carbon-cycle modelling results

The combined effect of the two different LGM ocean circulation patterns and the associated altered sea-surface boundary conditions on atmospheric carbon budgets is summarized in Table 2. The circulation-induced pCO_2 lowering is of comparable magnitude, amounting to 13.3 μatm in experiment LGMC and 16.0 μatm in experiment LGMW, respectively. These relatively small pCO_2 reductions agree with the findings of Winguth et al. (1999) who noted that the effect of changes in thermohaline circulation alone on pCO_2 is relatively small. In our model one reason for the relatively small drop in pCO_2 is a negative feedback linked to the biological "soft-tissue pump" (Volk and Hoffert, 1985). The glacial decrease in NADW production leads to an overall shift of phosphate, that is, the productivity-limiting nutrient, from the surface to the interior of the oceans. The globally integrated phosphate inventory decreases by ~5% in the uppermost model layer in both LGM experiments compared to the control run, resulting in a corresponding decrease in globally integrated export production of organic carbon by ~3% (Table 2). This weakening of the soft-tissue pump constitutes a negative feedback, which counteracts the circulation induced decrease in atmospheric pCO_2 (Marchal et al., 1998; Schulz et al., 2001). At the same time lowered glacial SST increase the production ratio of organic matter to calcareous shells ("rain ratio") by ~3%, which partly offsets the weaker soft-tissue pump via a weaker biological "carbonate pump" (Volk and Hoffert, 1985). The glacial reduction in atmospheric pCO_2 goes along with positive atmospheric $\Delta^{14}C$ anomalies of 18.9‰ (exp. LGMC)

Table 2
Characteristic quantities of the global carbon cycle in the three experiments

	CTRL	LGMC	LGMW
pCO_2 (μatm)	280	266.7	264
P_{org} (Gt C/year)	11.1	10.8	10.8
P_{carb} (Gt C/year)	1.25	1.19	1.18
P_{org}/P_{carb}	8.9	9.1	9.2

Atmospheric CO_2 content (pCO_2), globally integrated biological export production of organic carbon (P_{org}) and carbonate carbon (P_{carb}), and globally averaged "rain ratio".

and 20.0‰ (exp. LGMW). In contrast, atmospheric $\delta^{13}C$ decreases only marginally between −0.03‰ (exp. LGMC) and −0.04‰ (exp. LGMW).

The modelled $\delta^{13}C$ field in the Atlantic Ocean for the control experiment (Fig. 4a) clearly reflects the various water masses in this ocean basin: Newly produced NADW is characterized by $\delta^{13}C$ values greater than 0.8‰, extending from the surface of the northern North Atlantic (60–70°N) to 2.5-km depth near the equator. The NADW layer is sandwiched between two layers of relatively low $\delta^{13}C$ values, AABW at the bottom and Antarctic Intermediate Water near 1-km depth. Overall, the $\delta^{13}C$ distribution in the control experiment is in good agreement with the observed modern $\delta^{13}C$ distribution (cf. Kroopnick, 1985). The ^{14}C ages of the water masses (relative to the atmosphere) in the control experiment (Fig. 4b) show a general increase from north to south in the Atlantic Ocean, in agreement with observations (Östlund et al., 1987). In contrast to the observations, the model shows no clear delineation between young NADW and older AABW below. This deficit of the model probably results from the underestimation of the NADW penetration in the OGCM and the implicit vertical diffusion in the carbon-cycle model, which tends to weaken any pronounced vertical ^{14}C-age gradient in the Atlantic Ocean. A similar bias was also found in a study with a coarse-resolution OGCM that included ^{14}C as tracer (England and Rahmstorf, 1999).

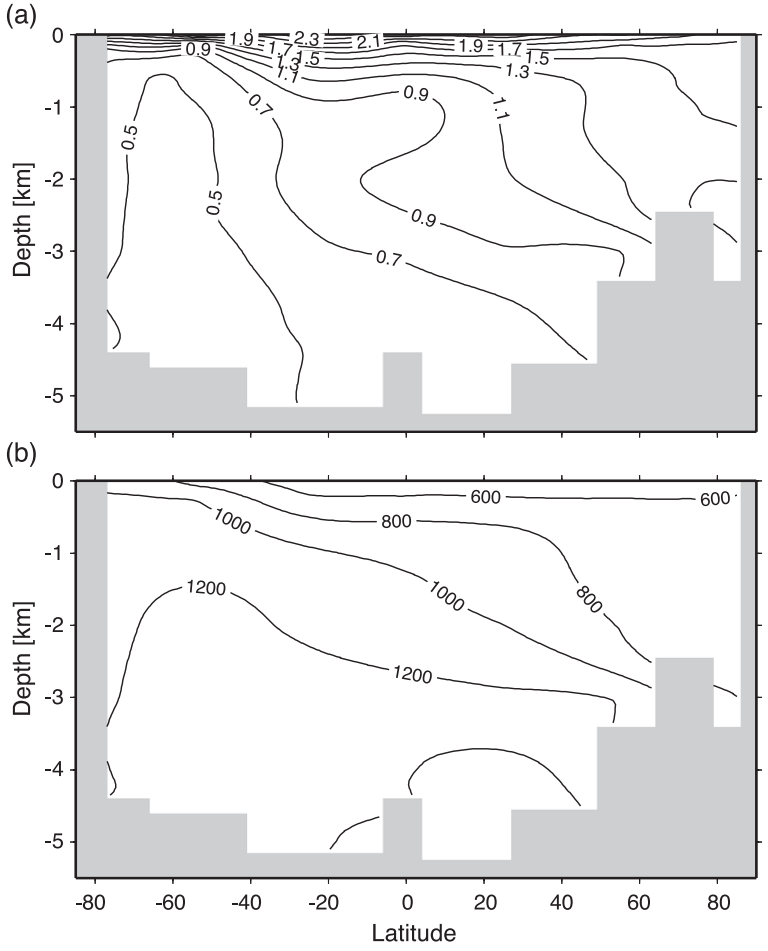

Fig. 4. Modern control experiment (CTRL). (a) $\delta^{13}C$ distribution in the Atlantic Ocean (contour interval = 0.2‰). (b) ^{14}C-ages (relative to the atmosphere) in the Atlantic Ocean (contour interval = 200 years).

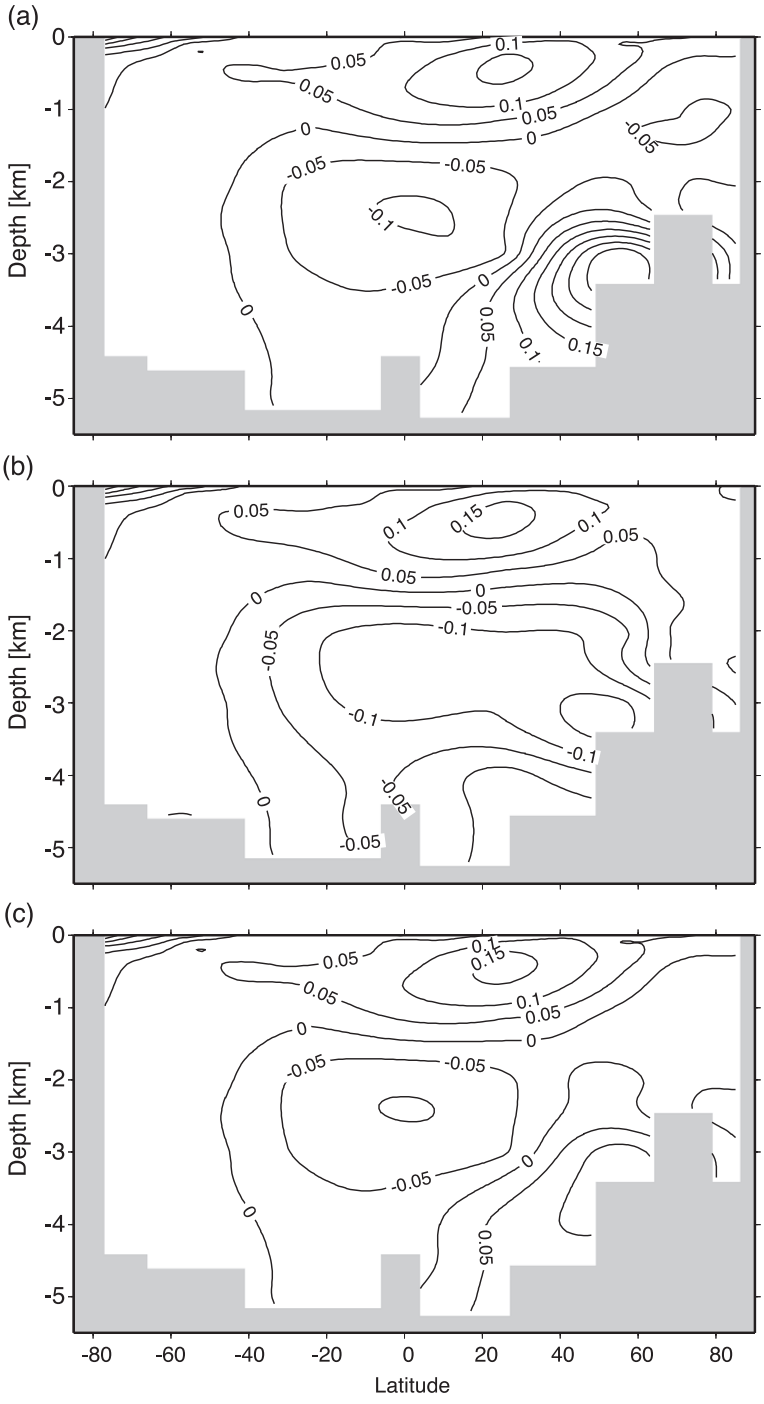

Fig. 5. Deviation of $\delta^{13}C$ distribution from experiment CTRL in the Atlantic Ocean for experiment (a) LGMC, (b) LGMW and (c) LGMS (contour interval = 0.05 ‰). See discussion for details of experiments LGMS.

For experiment LGMC the model predicted $\delta^{13}C$ anomalies in the Atlantic Ocean (north of 40°S) range from approximately −0.1‰ to 0.3‰ (Fig. 5a). Negative anomalies extend from the surface in the northern North Atlantic Ocean to the bottom south of the equator and are most pronounced at mid-depth in the equatorial Atlantic Ocean. A large positive $\delta^{13}C$ anomaly of 0.33‰ occurs at the southern flank of the Greenland-Scotland Ridge in approximately 3-km depth (Fig. 5a). Above 0.5–1.5-km depth, the entire Atlantic is characterized by positive $\delta^{13}C$ anomalies of up to 0.16‰ . The ^{14}C-age anomaly pattern in experiment LGMC (Fig. 6a) mirrors the corresponding $\delta^{13}C$ anomaly patterns. While most parts of the Atlantic Ocean show positive age anomalies, a distinct minimum of −160 years appears at the southern flank of the Greenland–Scotland Ridge, indicating a significantly better ventilation at this location than today. This model behaviour can be understood when considering the southward shift of the convection sites, that is, deep-water formation areas, between experiments CTRL (Fig. 3a) and LGMC (Fig. 3b): in the corresponding box stack of the carbon-cycle model the maximum convection depth increases from 0.85 to 2.5 km between experiments CTRL and LGMC. The enhanced glacial convection hampers the flow of

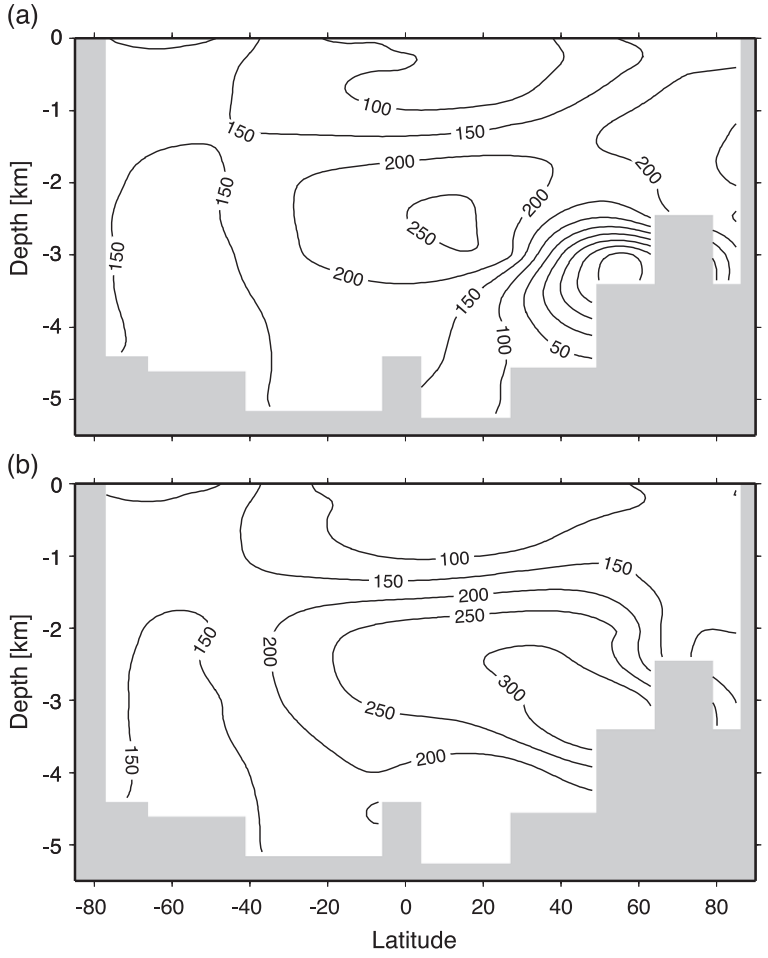

Fig. 6. Deviation of ^{14}C-ages (relative to the atmosphere) from experiment CTRL in the Atlantic Ocean for experiment (a) LGMC and (b) LGMW (contour interval = 50 years).

"old" AABW into this latitude belt, which drops from 1.1 Sv in the control run to 0.16 Sv in experiment LGMC and ensues the observed decrease in ^{14}C age.

Differences in $\delta^{13}C$ distribution and ^{14}C ages between experiments LGMW and LGMC are largest in the north Atlantic Ocean (cf. Figs. 5a,b and 6a,b), where the maximum $\delta^{13}C$ anomaly (0.33 ‰) in experiment LGMC at the Greenland–Scotland Ridge is replaced by a pronounced minimum anomaly of −0.16 ‰ (Fig. 5b). Similarly, the reduction in ^{14}C age in experiment LGMC vanishes in experiment LGMW and is replaced by a positive ^{14}C-age anomaly of 340 years (Fig. 6b). Again the convection pattern associated with the seasonally ice-free Nordic Seas in experiment LGMW (Fig. 3c) accounts for this model result since it allows for the advection of old, $\delta^{13}C$ depleted AABW into this model layer at a rate only slightly below the modern value of 1 Sv. Overall, the structure of the $\delta^{13}C$ anomaly pattern in experiment LGMW in the Atlantic Ocean exhibits a partition between negative anomalies south of the Greenland-Scotland Ridge and below 1.5 km and positive anomalies above this level and the entire Nordic Seas.

5. Discussion

Both modelled LGM circulation patterns are consistent with palaeoceanographic data with respect to a shallowing of the NADW layer and a more northerly penetration of AABW as compared to today (Boyle and Keigwin, 1987; Oppo and Fairbanks, 1987; Duplessy et al., 1988; Sarnthein et al., 1994). However, only the experiment with seasonally ice-free Nordic Seas (LGMW) agrees with the inferred deep-water formation north of Iceland during the LGM (Sarnthein et al., 1995; Weinelt et al., 1996). In both LGM experiments, the core of modelled NADW (not shown) appears ~0.8 km shallower than in the reconstruction of Sarnthein et al. (1994). As for the control experiment, we attribute this discrepancy to the low vertical resolution of the OGCM. Yu et al. (1996) postulated that NADW export to the Southern Ocean remained at its Holocene rate during the LGM. This contrasts with our model results, which indicate a weakening in glacial NADW export by 50% and are thus in better agreement with the reevaluation of the Yu et al. data by Marchal et al. (2000). For comparison, the decrease in NADW export obtained in some other OGCM studies ranges from 53% to 75% (Duplessy et al., 1996, 75%; Ganopolski et al., 1998, 66%; Weaver et al., 1998, 63%; Campin et al., 1999, 53%), estimated from the published zonally integrated meridional mass transport streamfunctions). Winguth et al. (1999) obtained an even stronger reduction by 83% in their inverse model.

The modelled glacial circulation patterns depend on the reconstructed surface boundary conditions, which are subject to considerable uncertainties. With respect to the large-scale overturning circulation, surface density in the deep-water formation areas at high-latitudes is of particular importance. Owing to the cold temperatures, seawater density in these regions is mainly controlled by variations in salinity. Based on a number of sensitivity experiments (Schäfer-Neth and Paul, 2001; Paul and Schäfer-Neth, 2003), we regard the employed sea-surface salinity pattern as the most likely out of a range of possible salinity fields. Further information on the robustness of the boundary conditions can be found in Schäfer-Neth and Paul (2001) and Paul and Schäfer-Neth (2003).

To further evaluate the difference between the two LGM experiments we turn to reconstructed $\delta^{13}C$ differences between the LGM and today, derived from measurements on benthic foraminifera. For the Atlantic Ocean, the data suggest a partitioning between positive anomalies above ~2-km depth and negative anomalies below this level (Fig. 7; see also Sarnthein et al., 1994). This anomaly pattern agrees better with the $\delta^{13}C$ anomalies of experiment LGMW (Fig. 5b) than of experiment LGMC (Fig. 5a). In particular, the positive anomalies which characterize the entire water column in the North Atlantic (>60 °N; Fig. 7) are only reproduced in experiment LGMW. Moreover, the positive $\delta^{13}C$ anomaly at the southern flank of the Greenland-Scotland Ridge in experiment LGMC (Fig. 5a) has no counterpart in the data-based anomalies. However, the boundary between positive and negative anomalies in the Atlantic Ocean appears ~0.8 km too shallow in experiment LGMW compared to the palaeoceanographic data. Whereas, the sign of the $\delta^{13}C$ anomalies in experiment LGMW are in overall agreement with the data, the model significantly underestimates the magnitude of the anomalies in the Atlantic Ocean by a factor up to eight near the

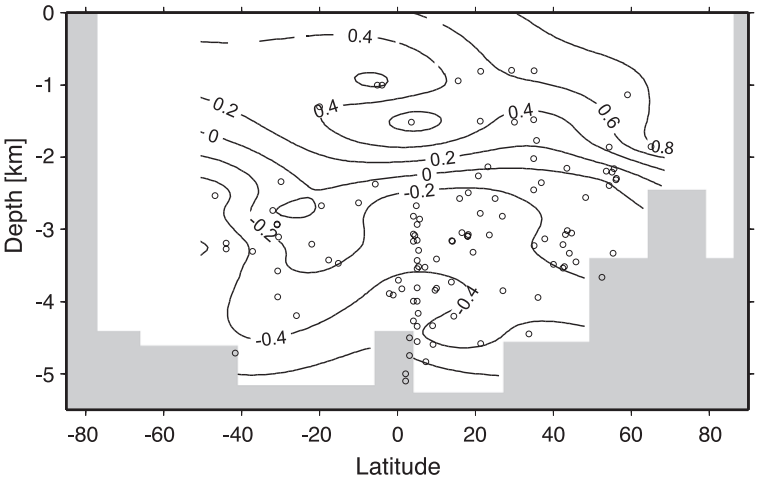

Fig. 7. Data-based $\delta^{13}C$ differences between LGM and today in the Atlantic Ocean (contour interval = 0.2 ‰). Measured epibenthic $\delta^{13}C$ data (circles; Curry et al., 1988; Sarnthein et al., 1988, 1994; Boyle, 1992) were mapped on the meridional sections irrespective of their longitudinal position. To account for a glacial–interglacial shift in oceanic $\delta^{13}C$ data, linked to the transfer of isotopically light terrestrial carbon, an offset of 0.35 ‰ was added to the anomalies (Duplessy et al., 1988; Crowley, 1995).

bottom. Based on an additional experiment with a further weakened glacial NADW production (not shown), a possible cause for this discrepancy may be that the glacial NADW production is still too large, leading to an overestimation of the smoothing effect of the oceanic overturning circulation on the vertical $\delta^{13}C$ gradients that originate primarily from the action of the biological soft-tissue pump.

To assess the effect of deep convection in the open North Atlantic Ocean in experiment LGMC (cf. Fig. 3a,b) on the modelled $\delta^{13}C$ distribution, we performed an additional sensitivity experiment (LGMS) in which the maximum depth of convection in the carbon-cycle box stack south of the Greenland–Scotland Ridge was restricted. Reducing convection depth by a single model level, that is, from 2.5- to 1.5-km depth, leads already to a dramatic reduction of the positive $\delta^{13}C$ in the deep North Atlantic Ocean (Fig. 5c) compared to experiment LGMC (Fig. 5a). Decreasing convection depth further to 0.85 km does not alter this new $\delta^{13}C$ anomaly pattern significantly (not shown). If in addition the explicit vertical water exchange is suppressed in accordance with the reduced convection depth, even a weak negative $\delta^{13}C$ anomaly (up to -0.1 ‰; not shown) appears. However, as for experiment LGMC, all three sensitivity experiments result in negative $\delta^{13}C$ anomalies at latitudes >60 °N and depth below ~1 km (Fig. 5c), a result which is in contrast to the palaeoceanographic data (Fig. 7).

Based on the sensitivity experiments, it seems likely that the CLIMAP (1981) based reconstruction in experiment LGMC leads to an overestimation of convection depth south of Iceland. While seasonal convection and deep-water formation in the Nordic Seas appear necessary to explain the reconstructed $\delta^{13}C$ anomalies in this region, we cannot rule out that convection south of Iceland was indeed more intensive, than predicted by the OGCM when forced with the Weinelt et al. (1996) sea-surface conditions.

The difference between ^{14}C ages measured on coexisting benthic and planktonic foraminifera ("ventilation age") serves as deep-water ventilation proxy and can be compared to the corresponding model predicted ^{14}C age differences (derived from the ^{14}C-age fields in Figs. 4b and 6). Measurements indicate that the ventilation age increased by 280 ± 95 years in the equatorial Atlantic Ocean (2.8–3.5-km depth) during the LGM compared to today (Broecker et al., 1990). The corresponding changes in the model amounts to 121 years in experiment LGMC and 211 years in experiment LGMW. (Taking into account that the water masses are shifted upward by ~ 0.8 km in the model, the anomalies are 145 and 207 years.) Hence, the results

of experiment LGMW are in better agreement with the observation than those of experiment LGMC.

6. Conclusions

Our sensitivity experiments indicate that ice-free conditions in the Nordic Seas during LGM summer (Weinelt et al., 1996) have an important effect on the circulation and carbon cycle in the Atlantic Ocean, compared to a situation with perennial sea-ice cover (CLIMAP, 1981). The better agreement between model results for seasonally ice-free conditions and palaeoceanographic reconstructions with respect to the location of deep-water formation areas, $\delta^{13}C$ distribution and ^{14}C ventilation ages in the North Atlantic Ocean lends further support to the sea-surface reconstruction of Weinelt et al. (1996). Thus, model and data substantiate the idea of reduced albeit active deep-water formation in the Nordic Seas during the LGM (cf. Sarnthein et al., 1994). Our results also suggest that the glacial sea-ice extent in the Nordic Seas is only of minor importance for understanding variations in atmospheric CO_2 concentration.

Acknowledgements

We greatly appreciate the constructive comments of two anonymous referees as well as the initial editorial handling by B. Turcq after the 31st IGC in 2000. The early stage of this work was supported by the German Klimaforschungsprogramm (MS) and Alexander v. Humboldt Stiftung (AP) and was mainly conducted while visiting the Scripps Institution of Oceanography. We thank W.H. Berger for his hospitality during our stay. The work was finalized within the framework of the DFG Research Center "Ocean Margins" (Publication RCOM0112).

References

Anderson, L.A., Sarmiento, J.L., 1994. Redfield ratios of remineralization determined by nutrient data analysis. Glob. Biogeochem. Cycles 8, 65–80.

Archer, D., Winguth, A., Lea, D., Mahowald, N., 2000. What caused the glacial/interglacial atmospheric pCO_2 cycles? Rev. Geophys. 38, 159–189.

Bacastow, R., Maier-Reimer, E., 1990. Ocean-circulation model of the carbon cycle. Clim. Dyn. 4, 95–125.

Barnola, J.M., Raynaud, D., Korotkevich, Y.S., Lorius, C., 1987. Vostok ice core provides 160,000-year record of atmospheric CO_2. Nature 329, 408–414.

Bolin, B. (Ed.), 1981. Carbon Cycle Modelling. Wiley, Chichester.

Boyle, E.A., 1988. The role of vertical fractionation in controlling late Quaternary atmospheric carbon dioxide. J. Geophys. Res. C93, 15701–15714.

Boyle, E.A., 1992. Cadmium and $\delta^{13}C$ paleochemical ocean distributions during the stage 2 glacial maximum. Annu. Rev. Earth Planet. Sci. 20, 245–287.

Boyle, E.A., Keigwin, L.D., 1987. North Atlantic thermohaline circulation during the past 20,000 years linked to high-latitude surface temperature. Nature 330, 35–40.

Broecker, W.S., Peng, T.-H., 1986. Glacial to interglacial changes in the operation of the glacial carbon cycles. Radiocarbon 28, 309–327.

Broecker, W.S., Peng, T.-S., Trumbore, S., Bonani, G., Wolfli, W., 1990. The distribution of radiocarbon in the glacial ocean. Glob. Biogeochem. Cycles 4, 103–117.

Brovkin, V., Hofmann, M., Bendtsen, J., Ganopolski, A., 2002. Ocean biology could control atmospheric $\delta^{13}C$ during glacial–interglacial cycle. G3 3 (10.1029/2001GC000270).

Bryan, K., Lewis, L.J., 1979. A water mass model of the world ocean circulation. J. Geophys. Res. 84, 2503–2517.

Campin, J.-M., Fichefet, T., Duplessy, J.-C., 1999. Problems with using radiocarbon to infer ocean ventilation rates for past and present climates. Earth Planet. Sci. Lett. 165, 17–24.

CLIMAP Project Members, 1981. Seasonal reconstructions of the Earth's surface at the Last Glacial Maximum. Map Chart Ser. (Geol. Soc. Am.) MC-36.

Crowley, T.J., 1995. Ige age terrestrial carbon changes revisited. Glob. Biogeochem. Cycles 9, 377–389.

Curry, W.B., Duplessy, J.-C., Labeyrie, L.D., Shackleton, N.J., 1988. Changes in the distribution of $\delta^{13}C$ of deep water ΣCO_2 between the last glaciation and the Holocene. Paleoceanography 3, 317–341.

Dickson, A.G., Millero, F.J., 1987. A comparison of the equilibrium constants for the dissociation of carbonic acid in seawater media. Deep-Sea Res. 34, 1733–1743.

Dugdale, R.C., 1967. Nutrient limitation in the sea: dynamics, identification, and significance. Limnol. Oceanogr. 12, 685–695.

Duplessy, J.C., Shackleton, N.J., Fairbanks, R.G., Labeyrie, L., Oppo, D., Kallel, N., 1988. Deepwater source variations during the last climatic cycle and their impact on the global deepwater circulation. Paleoceanography 3, 343–360.

Duplessy, J.-C., Labeyrie, L., Julliet-Lerclerc, A., Duprat, J., Sarnthein, M., 1991. Surface salinity reconstruction of the North Atlantic Ocean during the Last Glacial Maximum. Oceanol. Acta 14, 311–324.

Duplessy, J.C., Labeyrie, L., Paterne, M., Hovine, S., Fichefet, T., Duprat, J., Labracherie, M., 1996. High latitude deep water sources during the Last Glacial Maximum and the intensity of the global oceanic circulation. In: Wefer, G., Berger, W.H., Sie-

dler, G., Webb, D.J. (Eds.), The South Atlantic. Springer-Verlag, Berlin, pp. 445–460.

England, M.H., Rahmstorf, S., 1999. Sensitivity of ventilation rates and radiocarbon uptake to subgrid-scale mixing in ocean models. J. Phys. Oceanogr. 29, 2802–2827.

Falkowski, P.G., Scholes, R.J., Boyle, E., Candell, J., Canfield, D., Elser, J., Gruber, N., Hibbard, K., Högberg, P., Linder, S., Mackenzie, F.T., Moore III, B., Pedersen, T., Rosenthal, Y., Seitzinger, S., Smetacek, V., Steffen, W. 2000. The global carbon cycle: a test of our knowledge of Earth as a system. Science 290, 291–296.

Farrow, D.E., Stevens, D.P., 1995. A new tracer advection scheme for Bryan and Cox type ocean general circulation models. J. Phys. Oceanogr. 25, 1731–1741.

Ganopolski, A., Rahmstorf, S., Petoukhov, V., Claussen, M., 1998. Simulation of modern and glacial climates with a coupled global model of intermediate complexity. Nature 391, 351–356.

Heimann, M., Monfray, P., 1989. Spatial and temporal variation of the gas exchange coefficient for CO_2: 1. Data analysis and global validation. Rep.-Max-Planck-Inst. Meteorol. 31, 1–29.

Heinze, C., 1990. Zur Erniedrigung des atmosphärischen Kohlendioxidgehalts durch den Weltozean während der letzten Eiszeit. Exam.arb.-Max-Planck-Inst. Meteorol., Hambg. 3, 1–180.

Hewitt, C.D., Broccoli, A.J., Mitchell, J.F.B., Stouffer, R.J., 2001. A coupled model study of the Last Glacial Maximum: was part of the North Atlantic relatively warm? Geophys. Res. Lett. 28, 1571–1574.

Iglesias-Rodriguez, M.D., Armstrong, R., Feely, R., Hood, R., Kleypas, J., Milliman, J.D., Sabine, C., Sarmiento, J., 2002. Progress made in study of ocean's calcium carbonate budget. EOS Trans. AGU 83 (34), 365–375.

Jasper, J.P., Hayes, J.M., Mix, A.C., Prahl, F.G., 1994. Photosynthetic fractionation of ^{13}C and concentrations of dissolved CO_2 in the central equatorial Pacific during the last 255,000 years. Paleoceanography 9, 781–798.

Johns, T.C., Carnell, R.E., Crossley, J.F., Gregory, J.M., Mitchell, J.F.B., Senior, C.A., Tett, S.F.B., Wood, R.A., 1997. The second Hadley Centre coupled ocean-atmosphere GCM: model description, spinup and validation. Clim. Dyn. 13, 103–134.

Johnson, K.M., Körtzinger, A., Mintrop, L., Duinker, J.C., Wallace, D.W.R., 1999. Coulometric total carbon dioxide analysis for marine studies: measurement and internal consistency of underway TCO_2 concentrations. Mar. Chem. 67, 123–144.

Keeling, C.D., Bolin, B., 1967. The simultaneous use of chemical tracers in oceanic studies: I. General theory of reservoir models. Tellus 19, 566–581.

Keir, R.S., 1988. On the late Pleistocene ocean chemistry and circulation. Paleoceanography 3, 413–445.

Keir, R.S., 1990. Reconstructing the ocean carbon system variation during the last 150,000 years according to the Antarctic nutrient hypothesis. Paleoceanography 5, 253–276.

Kim, S.-J., Flato, G.M., Boer, G.J., McFarlane, N.A., 2002. A coupled climate model simulation of the Last Glacial Maximum: Part 1. Transient multi-decadal response. Clim. Dyn. 19, 515–537.

Kroopnick, P.M., 1985. The distribution of ^{13}C of $\sum CO_2$ in the world oceans. Deep-Sea Res. 32, 57–84.

Lalli, C.M., Parsons, T., 1993. Biological Oceanography. Pergamon, Oxford.

Levitus, S., Burgett, R., Boyer, T.P., 1994. World Ocean Atlas 1994, vol. 3. NOAA Natl. Environ. Satell. Data and Inf. Ser., Washington, DC. Salinity.

Lorenz, S., Grieger, B., Helbig, P., Herterich, K., 1996. Investigating the sensitivity of the atmospheric general circulation model ECHAM 3 to paleoclimatic boundary conditions. Geol. Rundsch. 85, 513–524.

Maier-Reimer, E., Mikolajewicz, U., Hasselmann, K., 1993. Mean circulation of the Hamburg LSG OGCM and its sensitivity to the thermohaline surface forcing. J. Phys. Oceanogr. 23, 731–757.

Marchal, O., Stocker, T.F., Joos, F., 1998. Impact of oceanic reorganizations on the ocean carbon cycle and atmospheric carbon dioxide content. Paleoceanography 13, 225–244.

Marchal, O., Francois, R., Stocker, T.F., Joos, F., 2000. Ocean thermohaline circulation and sedimentary $^{231}Pa/^{230}Th$ ratio. Paleoceanography 15, 625–641.

Melles, M., 1991. Late Quaternary paleoglaciology and paleoceanography at the continental margin of the southern Weddell Sea, Antarctica. Ber. Polarforsch. 81, 1–190.

Najjar, R.G., Sarmiento, J.L., Toggweiler, J.R., 1992. Downward transport and fate of organic matter in the ocean: simulations with a general circulation model. Glob. Biogeochem. Cycles 6, 45–76.

Oeschger, H., Siegenthaler, U., Schotterer, U., Gugelmann, A., 1975. A box diffusion model to study carbon dioxide exchange in nature. Tellus 27, 168–192.

Oppo, D.W., Fairbanks, R.G., 1987. Variability in the deep and intermediate water circulation of the Atlantic Ocean during the past 25,000 years: Northern hemisphere modulation of the Southern Ocean. Earth Planet. Sci. Lett. 86, 1–15.

Östlund, H.G., Craig, H., Broecker, W.S., Spenncer, D. (Eds.), 1987. GEOSECS Atlantic, Pacific, and Indian Ocean Expeditions, vol. 7. National Science Foundation, Washington, DC.

Paul, A., Schäfer-Neth, C., 2003. Modeling the water masses of the Atlantic Ocean at the Last Glacial Maximum. Paleoceanography 18, 1058 (10.1029/2002PA000783).

Peng, T.-H., Takahashi, T., Broecker, W.S., Olaffson, J., 1987. Seasonal variability of carbon dioxide, nutrients and oxygen in the northern North Atlantic surface water: observations and a model. Tellus 39B, 439–458.

Sarnthein, M., Winn, K., Duplessy, J.-C., Fontugne, M.R., 1988. Global variations of surface ocean productivity in low and mid latitudes: influence on CO_2 reservoirs of the deep ocean and atmosphere during the last 21,000 years. Paleoceanography 3, 361–399.

Sarnthein, M., Winn, K., Jung, S.J.A., Duplessy, J.C., Labeyrie, L., Erlenkeuser, H., Ganssen, G., 1994. Changes in East Atlantic deepwater circulation over the last 30,000 years—8 time slice reconstructions. Paleoceanography 9, 209–267.

Sarnthein, M., Jansen, E., Weinelt, M., Arnold, M., Duplessy, J.C., Erlenkeuser, H., Flatoy, A., Johannessen, G., Johannessen, T., Jung, S., Koc, N., Labeyrie, L., Maslin, M., Pflaumann, U., Schulz, H., 1995. Variations in Atlantic surface ocean paleoceanography, 50°–80°N: a time-slice record of the last 30,000 years. Paleoceanography 10, 1063–1094.

Sarnthein, M., Stattegger, K., Dreger, D., Erlenkeuser, H., Grootes, P., Haupt, B.J., Jung, S., Kiefer, T., Kuhnt, W., Pflaumann, U., Schäfer-Neth, C., Schulz, H., Schulz, M., Seidov, D., Simstich, J., van Kreveld, S., Vogelsang, E., Völker, A., Weinelt, M., 2001. Fundamental modes and abrupt changes in North Atlantic circulation and climate over the last 60 ky—concepts, reconstructions and numerical modeling. In: Schäfer, W., Ritzrau, W., Schlüter, M., Thiede, J. (Eds.), The Northern North Atlantic: A Changing Environment. Springer-Verlag, Berlin, pp. 365–410.

Schäfer-Neth, C., Paul, A., 2001. Circulation of the glacial Atlantic: a synthesis of global and regional modeling. In: Schäfer, P., Ritzrau, W., Schlüter, M., Thiede, J. (Eds.), The Northern North Atlantic: A Changing Environment. Springer-Verlag, Berlin, pp. 441–462.

Schmitz, W.J., 1995. On the interbasin-scale thermohaline circulation. Rev. Geophys. 33, 151–173.

Schulz, M., Seidov, D., Sarnthein, M., Stattegger, K., 2001. Modeling ocean–atmosphere carbon budgets during the Last Glacial Maximum—Heinrich 1 meltwater event—Bölling transition. Int. J. Earth Sci. 90, 412–425.

Seidov, D., Haupt, B.J., 1999. Numerical study of glacial and meltwater global ocean thermohaline conveyor. In: Harff, J., Lemke, W., Stattegger, K. (Eds.), Computerized Modeling of Sedimentary Systems. Springer-Verlag, Berlin, pp. 79–113.

Seidov, D., Sarnthein, M., Stattegger, K., Prien, R., Weinelt, M., 1996. North Atlantic ocean circulation during the Last Glacial Maximum and subsequent meltwater event: a numerical model. J. Geophys. Res. C101, 16305–16332.

Shea, D.J., Trenberth, K.E., Reynolds, R.W., 1990. A global monthly sea surface temperature climatology. NCAR Tech. Note TN-345, 1–167.

Siegenthaler, U., Wenk, T., 1984. Rapid atmospheric CO_2 variations and ocean circulation. Nature 308, 624–626.

Sigman, D.M., Boyle, E.A., 2000. Glacial/interglacial variations in atmospheric carbon dioxide. Nature 407, 859–869.

Stephens, B.B., Keeling, R.F., 2000. The influence of Antarctic sea ice on glacial–interglacial CO_2 variations. Nature 404, 171–174.

Stocker, T.F., Broecker, W.S., Wright, D.G., 1994. Carbon uptake experiments with a zonally-averaged global ocean circulation model. Tellus 46B, 103–122.

Takahashi, T., Broecker, W.S., Bainbridge, A.E., 1981. The alkalinity and total carbon dioxide concentration in the world oceans. In: Bolin, B. (Ed.), Carbon Cycle Modelling. Wiley, Chichester, pp. 271–286.

Toggweiler, J.R., 1999. Variation of atmospheric CO_2 by ventilation of the ocean's deepest water. Paleoceanography 14, 571–588.

Volk, T., Hoffert, M.I., 1985. Ocean carbon pumps: analysis of relative strengths and efficiencies in ocean-driven atmospheric CO_2 changes. In: Sundquist, E.T., Broecker, W.S. (Eds.), The carbon cycle and atmospheric CO_2: natural variations Archean to present. American Geophysical Union, Washington, DC, pp. 99–110.

Weaver, A.J., Eby, M., Augustus, F.F., Wiebe, E.C., 1998. Simulated influence of carbon dioxide, orbital forcing and ice sheets on the climate of the Last Glacial Maximum. Nature 394, 847–853.

Weinelt, M., Sarnthein, M., Pflaumann, U., Schulz, H., Jung, S., Erlenkeuser, H., 1996. Ice-free Nordic Seas during the Last Glacial Maximum? Potential sites of deepwater formation. Palaeoclimatology 1, 283–309.

Winguth, A.M.E., Archer, D., Duplessy, J.C., Maier-Reimer, E., Mikolajewicz, U., 1999. Sensitivity of paleonutrient tracer distributions and deep-sea circulation to glacial boundary conditions. Paleoceanography 14, 304–323.

Yu, E.F., Francois, R., Bacon, M.P., 1996. Similar rates of modern and last-glacial ocean thermohaline circulation inferred from radiochemical data. Nature 379, 689–694.

Zhang, J., Quay, P.D., Wilbur, D.O., 1995. Carbon isotope fractionation during gas–water exchange and dissolution of CO_2. Geochim. Cosmochim. Acta 59, 107–114.